The density and polarization of an ion-dipole-electrolyte near a charged wall

Enrique Díaz-Herrera and F. Forstmann

Citation: The Journal of Chemical Physics **102**, 9005 (1995); doi: 10.1063/1.468849
View online: http://dx.doi.org/10.1063/1.468849
View Table of Contents: http://scitation.aip.org/content/aip/journal/jcp/102/22?ver=pdfcov
Published by the AIP Publishing

Articles you may be interested in

Production of Polarized Ions with Nearly Resonant Charge-Exchange Collisions in Plasma
AIP Conf. Proc. **980**, 209 (2008); 10.1063/1.2888089

Structure of the dipolar hard sphere fluid near a charged hard wall: Density profile and polarization
J. Chem. Phys. **90**, 4491 (1989); 10.1063/1.456636

A theoretical study of the solid–electrolyte solution interface. I. Structure of a hard sphere ion–dipole mixture near an uncharged hard wall
J. Chem. Phys. **89**, 4994 (1988); 10.1063/1.455643

Polarization density profiles for dipoles against an electrified wall in the MS and RLHNC approximations
J. Chem. Phys. **75**, 5497 (1981); 10.1063/1.441953

The structure of electrolytes at charged surfaces: Ion–dipole mixtures
J. Chem. Phys. **73**, 2949 (1980); 10.1063/1.440468

This article is copyrighted as indicated in the article. Reuse of AIP content is subject to the terms at: http://scitation.aip.org/termsconditions. Downloaded to IP: 148.206.45.218 On: Tue, 14 Jul 2015 15:03:15

The density and polarization of an ion-dipole-electrolyte near a charged wall

Enrique Díaz-Herrera
Departamento de Física, Universidad Autónoma Metropolitana-Iztapalapa, Avenida Michoacán y Purisima s/n, Apartado Postal 55-542, 09340 D. F., México

F. Forstmann
Institut für Theoretische Physik, Freie Universität Berlin, Arnimallee 14, D-14195 Berlin, Germany

(Received 14 February 1995; accepted 10 March 1995)

The structure of the hard sphere dipolar liquid and the electrolyte with added hard sphere ions near a charged hard planar electrode has been investigated with the reference hypernetted chain integral equation (RHNC). We find a decrease of the dielectric function ϵ near the wall, a decrease of ϵ in the fluid due to saturation, a field dependent change in the dipole density near the wall, and a decrease of the ion density near the electrode due to solvation. Related to the demixing instability of the ion-dipole mixture, the ions suddenly concentrate near the surface at higher fields and lead to a sharp increase in the differential capacitance. Also electrostriction in the pure dipolar liquid with a field in the bulk is considered. © *1995 American Institute of Physics*.

I. INTRODUCTION

The structure of the double layer near an electrode determines its capacitance and charge transfer properties. Since the Poisson–Boltzmann approach by Gouy and Chapman,[1,2] there have been many attempts to build structural models,[3] e.g., including a distance of closest approach for ions, the Stern layer, introducing layers with different dielectric constants, usually lower ϵ closer to the electrode,[4,5] or even contemplating water clusters with compensated dipole moments.[6] Especially for the capacitance, the contribution from the metal surface has also been modeled.[7–9]

The methods of statistical mechanics have been applied more recently: Monte Carlo (MC) or molecular dynamics (MD) simulations[10,11] as well as integral equation calculations like hypernetted chain (HNC) or extensions of it. We concentrate on the latter, because our method of investigation is also an integral equation version. The investigation of the double layer with integral equations started when Blum and Henderson[12,13] formulated the Henderson–Abraham–Barker[14] equations for Coulomb interactions. During the following ten years, mainly the correction of the Gouy–Chapman theory due to finite ion sizes was investigated using the primitive model of an electrolyte, i.e., hard sphere ions.[15–26] Because many details of the double layer structure are due to solvent properties as well as to ion interactions, more sophisticated electrolyte models are required. Before one really comes to the solvent water with its complicated molecular structure and hydrogen bonds, some essential solvation properties can be studied with hard sphere dipoles as the solvent. This is the object of this article.

The hard sphere dipolar liquid has been studied earlier by Wertheim[27,28] and Høy and Stell[29,30] and the mean spherical approximation (MSA) of the integral equations has been solved exactly.[31] Near the surface Isbister and Freasier[32] evaluated MSA approximations. Later in linearized (LHNC)[33] and quadratic (QHNC)[34] approximations the angular dependent dipole interaction was considered small and was expanded in the HNC closure. This is not good enough for the magnitude of dipole moments like those in water or other solvents. An important step forward was made by Fries and Patey[35] and by Caillol[36] in treating the angular dependencies in the exponent of the HNC closure by bringing it down by a derivative. Now only the total and direct correlation functions need expansions in spherical harmonics, not the exponential in addition. Applications of this method have been made to homogeneous dipolar liquids[35,37] and electrolytes.[38,39] Also an interface has been approached by treating a mixture containing spheres with very large radii, neutral as well as charged.[40] These large spheres are then increased and the distributions of the smaller dipoles near the large sphere are considered to approach those in front of a planar wall. This limiting process apparently meets some convergence problems.[40] Also a solvent model containing an additional quadrupole moment has been treated in this way.[41–43] More recently Dong *et al*.[44] calculated the distribution of hard sphere dipoles and hard sphere ions in front of a planar uncharged wall. Very recently the interaction of a dipole model with the metal electrons has been considered.[45] We present here results for the uncharged as well as for the charged surface for the pure hard sphere dipolar fluid and for the ion-dipole mixture electrolyte.

In Sec. II we describe the electrolyte model and in Sec. III we outline the method of calculation. Section IV gives the results and a discussion for the pure dipolar fluid which does not show screening of an applied field. Section V discusses the results for the ion-dipole mixture. The effects of electrostriction are considered in Sec. VI. Some conclusions are summarized in Sec. VII.

II. THE MODEL AND THE METHOD OF CALCULATION

Our electrolyte is a mixture of hard sphere ions of diameter σ with charges $\pm q$ in the center and solvent particles modeled as hard spheres of the same diameter σ with a central dipole moment $\boldsymbol{\mu}$. The interaction potentials $u_{\alpha,\beta}(1,2)$ between particle of species α at 1 and β at 2, where for

This article is copyrighted as indicated in the article. Reuse of AIP content is subject to the terms at: http://scitation.aip.org/termsconditions. Downloaded to IP:

 0021-9606/95/102(22)/9005/13/$6.00 © 1995 American Institute of Physics

TABLE I. Parameters defining the system.

Parameter	in reduced dimensions
μ: dipole moment	$\mu^{\star 2}=\beta(\mu^2/\sigma^3)$
q: ion charge	$q^{\star 2}=\beta(q^2/\sigma^3)$
ω: surface charge density	$\omega^{\star}=\omega\sigma^2/e$
ρ_d: dipole density	$\rho_d^{\star}=\rho_d\sigma^3$
ρ_i: ion density	$\rho_i^{\star}=\rho_i\sigma^3$
T: temperature and $\beta=1/k_BT$	
σ: diameter of ions and dipoles	

dipoles the coordinates $i=(\mathbf{r}_i,\omega_i)$ include in addition to the position $\mathbf{r}_i$ the dipole orientation $\omega_i=(\theta_i,\varphi_i)$, are for $|\mathbf{r}_2-\mathbf{r}_1|>\sigma$:

$$\text{ion–ion:}\quad u_{+\pm}(1,2)=\pm\frac{1}{4\pi\epsilon_0}\frac{q^2}{|\mathbf{r}_2-\mathbf{r}_1|}, \tag{1}$$

$$\text{ion–dipole:}\quad u_{\pm d}(1,2)=\mp\frac{1}{4\pi\epsilon_0}\frac{q\boldsymbol{\mu}\cdot(\mathbf{r}_2-\mathbf{r}_1)}{|\mathbf{r}_2-\mathbf{r}_1|^3}, \tag{2}$$

dipole–dipole:

$$u_{dd}(1,2)=-\frac{1}{4\pi\epsilon_0}\left(\frac{3[\boldsymbol{\mu}_1\cdot(\mathbf{r}_2-\mathbf{r}_1)][\boldsymbol{\mu}_2\cdot(\mathbf{r}_2-\mathbf{r}_1)]}{|\mathbf{r}_2-\mathbf{r}_1|^5}-\frac{\boldsymbol{\mu}_1\boldsymbol{\mu}_2}{|\mathbf{r}_2-\mathbf{r}_1|^3}\right), \tag{3}$$

and, for $|\mathbf{r}_2-\mathbf{r}_1|<\sigma$, $u_{\alpha\beta}(1,2)=+\infty$.

We measure all our lengths in units of σ. Because all interactions are weighted in their proportion to kT, we have the following parameters, which define our system (see Table I).

The electrode wall at $z=0$ is infinitely hard, the particle centers can approach up to $z=\sigma/2$:

$$v_\alpha(z)=\infty \quad \text{for} \quad z<\frac{\sigma}{2}. \tag{4}$$

A homogeneous surface charge density ω leads for $z>\sigma/2$ to the interactions

$$\text{wall–ion:}\quad v_\pm(z)=\pm q\varphi^{\text{ex}}(z)=\pm q\ (-\epsilon_0^{-1}\omega\ z+\varphi_0), \tag{5}$$

$$\text{wall–dipole:}\quad v_d(z)=-\mu\ E_z^{\text{ex}}(z)\ \cos\theta=-\mu\ (\epsilon_0^{-1}\omega)\ \cos\theta\ . \tag{6}$$

We will also consider the uncharged wall $\omega=0$. With these interactions the resulting densities are translationally invariant parallel to the surface and depend therefore only on the distance z from the wall. The orientational dependence of the dipole density has cylindrical symmetry around the surface normal and therefore only the angle θ between dipole direction and surface normal shows up as a variable.

We neglect image interactions which are expected in front of a metal electrode. These interactions make the particle–particle potential dependent on the distance from the wall a severe complication. A recent integral equation study[46] showed that inclusion of the interactions of a particle with all the images of the other particles leads to results very close to those for totally neglecting the image interactions, while inclusion of only the own image of a particle, which could be easily handled as a surface potential, gives completely wrong results. Therefore neglecting images is a reasonable approximation.

III. THE METHOD OF CALCULATING THE PARTICLE DISTRIBUTIONS

We calculate the particle densities as well as the orientational distributions for the dipoles from integral equations derived by density functional arguments.[23,47–49] We use the hypernetted chain approximation (HNC) to these equations and include some additional repulsive wall-particle potential derived by Rosenfeld,[50] which leads to an agreement with simulations at the uncharged electrode. It improves the approximate treatment of the short ranged hard core interactions similar to the additional effective potentials in a "reference hypernetted chain" (RHNC) approximation in the bulk.[51,52] The densities are calculated from the set of equations

$$\ln\left[\frac{\rho_\alpha(1)}{\rho_\alpha^B}\right]=-\beta v_\alpha(1)+\sum_\gamma\int d2\,[\rho_\gamma(2)-\rho_\gamma^B]c_{\gamma\alpha}(2,1)-B(1)\ . \tag{7}$$

The direct particle–particle correlation functions $c_{\alpha\beta}(1,2)$ are calculated for the homogeneous electrolyte in the RHNC approximation as outlined in Refs. 53 and 54. The approximate wall-particle bridge functions $B(1)$ are taken equal for ions and dipoles and are given by the analytical expression from Ref. 50:

$$B(z_1)=A[(z_1-z_0)^3+3(z_1-z_0)^2]. \tag{8}$$

We have adjusted the two parameters A and z_0, until our integral equation results for the reference system, i.e., hard spheres at a hard wall, agreed with the Monte Carlo simulations by Levesque *et al.*[10] The optimal values are $A=11/4$ and $z_0=0.45$.

Equation (7) will be used to calculate the ion $(\alpha=+,-)$ density profiles

$$\ln\left[\frac{\rho_\pm(z_1)}{\rho_\pm^B}\right]=-\beta v_\pm(z_1)-B(z_1)+\frac{1}{4\pi}\int d\mathbf{r}_2\ d\omega_2\ [\rho_d(z_2,\theta_2)-\rho_d^B]\ c_{\pm d}(r_{12}\ \omega_2\ \omega_{12})+\sum_{\gamma=+,-}\int d\mathbf{r}_2\ [\rho_\gamma(z_2)-\rho_\gamma^B]c_{\pm\gamma}(r_{12})\ . \tag{9}$$

The density profile as well as the orientation distribution for the dipoles are calculated with

This article is copyrighted as indicated in the article. Reuse of AIP content is subject to the terms at: http://scitation.aip.org/termsconditions. Downloaded to IP:

$$\ln\left[\frac{\rho_d(z_1,\theta_1)}{\rho_d^B}\right]=-\beta v_d(z_1,\theta_1)-B(z_1)$$
$$+\frac{1}{4\pi}\int d\mathbf{r}_2\, d\omega_2\,[\rho_d(z_2,\theta_2)-\rho_d^B]$$
$$\times c_{dd}(r_{12}\ \omega_1\ \omega_2\ \omega_{12})$$
$$+\sum_{\gamma=+,-}\int d\mathbf{r}_2\,[\rho_\gamma(z_2)-\rho_\gamma^B]c_{d\gamma}(r_{12}\ \omega_1\ \omega_{12})\ . \qquad (10)$$

In order to solve this equation the angular dependent bulk direct correlation functions must be expanded into a basis set of rotational invariants $\Phi^{l_1l_2l}(\omega_1,\omega_2,\omega_{12})$, which are a linear combination of spherical harmonics:[55]

$$\Phi^{l_1l_2l}(\omega_1,\omega_2,\omega_{12})=\sum_{\lambda_1\lambda_2\lambda}C(l_1l_2l;\lambda_1\lambda_2\lambda)$$
$$\times\frac{4\pi}{\sqrt{2l_1+1}\sqrt{2l_2+1}}(-1)^\lambda$$
$$\times Y_{l_1\lambda_1}(\omega_1)Y_{l_2\lambda_2}(\omega_2)Y_{l\underline{\lambda}}(\omega_{12}), \qquad (11)$$

where $\Phi^{l_1l_2l}(\omega_1,\omega_2,\omega_{12})$ is a rotational invariant specialized for linear molecules and $C(l_1l_2l;\lambda_1\lambda_2\lambda)$ are the Clebsch–Gordan coefficients. In front of the wall the density profiles depend only on the distance z from the wall. In addition to z the dipole density is also a function of the dipole orientation, measured by the angle θ with respect to the surface normal because of the cylindrical symmetry. The dipole distribution can be expanded in a series of Legendre polynomials

$$\rho_d(1)=\rho_d(z,\theta)=\sum_{l=0}^{l_{\max}}\rho_d^l(z)\ p_l(\cos\theta)\ . \qquad (12)$$

We now use the expansions [Eqs. (11) and (12)] in Eqs. (9) and (10) and perform the angular integration.

As usual in coulombic systems it is appropriate to extract from the direct correlation functions the long-range part by

$$c_{\alpha\gamma}(r_{12})=c_{\alpha\gamma}(r_{12})^{\mathrm{SR}}-\beta u_{\alpha\gamma}(r_{12})\Theta(r_{12}-\sigma), \qquad (13)$$

where

$$\Theta(r_{12}-\sigma)=\begin{cases}0 & r_{12}<\sigma\\ 1 & r_{12}>\sigma\end{cases}. \qquad (14)$$

By the step function we avoid the singularity to be introduced into the short-range direct correlation function $c_{\alpha\gamma}(r_{12})^{\mathrm{SR}}$. The step function is convenient because we solve the integral equation system in r space. After including the separation Eq. (13) in Eqs. (9) and (10), we collect the long-range parts together with the external field to a resulting mean field $\varphi(z_1)$ and $E_z(z_1)$, which are respectively the mean electrostatic potential and the z component of the electric field intensity inside a cavity with diameter σ. The integration parallel to the surface can be done separately which leads to the definition of some short-range functions:

$$c_{\alpha\gamma}(z_2-z_1)_\parallel=\int_{|z_2-z_1|}^\infty dr_{12}\ r_{12}\ c_{\alpha\gamma}(r_{12})^{\mathrm{SR}},$$
$$c_{\alpha d}^{0ll}(z_2-z_1)_\parallel=\int_{|z_2-z_1|}^\infty dr_{12}\ r_{12}\ c_{\alpha d}^{0ll}(r_{12})^{\mathrm{SR}}\ p_l(\cos\theta_{12}),$$
$$c_{dd}^{mnl}(z_2-z_1)_\parallel=\int_{|z_2-z_1|}^\infty dr_{12}\ r_{12}\ c_{dd}^{mnl}(r_{12})^{\mathrm{SR}}\ p_l(\cos\theta_{12}), \qquad (15)$$
$$c_{d\gamma}^{l0l}(z_2-z_1)_\parallel=(-1)^l\int_{|z_2-z_1|}^\infty dr_{12}\ r_{12}$$
$$\times c_{\gamma d}^{0ll}(r_{12})^{\mathrm{SR}}\ p_l(\cos\theta_{12})\ .$$

Finally we obtain a system of coupled integral equations for the ion densities

$$\ln\left[\frac{\rho_\pm(z_1)}{\rho_\pm^B}\right]=-\beta\,[\pm q\ \varphi(z_1)]-B(z_1)+\sum_l\frac{1}{2}\sqrt{\frac{4\pi}{2l+1}}$$
$$\times\int_{-\infty}^\infty dz_2\,[\rho_d^l(z_2)-\rho_d^B]\ c_{\pm d}^{0ll}(z_2-z_1)_\parallel$$
$$+2\pi\sum_{\gamma=+,-}\int_{-\infty}^\infty dz_2\,[\rho_\gamma(z_2)-\rho_\gamma^B]$$
$$\times c_{\pm\gamma}(z_2-z_1)_\parallel, \qquad (16)$$

and the dipole density

$$\ln\left[\frac{\Sigma_l\rho_d^l(z_1)\ p_l(\cos\theta_1)}{\rho_d^B}\right]$$
$$=-\beta\,[-\mu\ E_z(z_1)\ \cos\theta_1]-B(z_1)+\sum_{mnl}\frac{2\pi}{2n+1}$$
$$\times\sqrt{\frac{2l+1}{4\pi}}\,C(mnl;000)\int_{-\infty}^\infty dz_2\,[\rho_d^n(z_2)-\rho_d^B]$$
$$\times c_{dd}^{mnl}(z_2-z_1)_\parallel p_m(\cos\theta_1)+2\pi\sum_l\sqrt{\frac{2l+1}{4\pi}}$$
$$\times\sum_{\gamma=+,-}\int_{-\infty}^\infty dz_2\,[\rho_\gamma(z_2)-\rho_\gamma^B]$$
$$\times c_{d\gamma}^{l0l}(z_2-z_1)_\parallel p_l(\cos\theta_1), \qquad (17)$$

where for $z>3\sigma/2$:

$$\varphi(z_1)=\varphi_q(z_1)+\varphi_d(z_1), \qquad (18)$$

$$E_z(z_1)=E_q(z_1)+E_d(z_1) \qquad (19)$$

with

This article is copyrighted as indicated in the article. Reuse of AIP content is subject to the terms at: http://scitation.aip.org/termsconditions. Downloaded to IP:

$$\varphi_q(z_1) = -\frac{\omega}{\epsilon_0} z_1 - \frac{1}{\epsilon_0}\int_0^\infty dz_2\, z_2\, q(z_2) + \frac{1}{\epsilon_0}\int_0^{z_1} dz_2 \times (z_2 - z_1)\, q(z_2) - \frac{1}{2\epsilon_0}\int_{z_1-\sigma}^{z_1+\sigma} dz_2\, q(z_2) \times (\sigma - |z_2 - z_1|), \tag{20}$$

$$\varphi_d(z_1) = -\frac{1}{\epsilon_0}\int_{z_1}^\infty dz_2\, P(z_2) - \frac{1}{2\epsilon_0}\int_{z_1-\sigma}^{z_1+\sigma} dz_2\, P(z_2)\left[\frac{(z_2-z_1)}{\sigma} - \frac{(z_2-z_1)}{|z_2-z_1|}\right] \tag{21}$$

and

$$E_q(z_1) = \frac{\omega}{\epsilon_0} + \frac{1}{\epsilon_0}\int_0^{z_1} dz_2\, q(z_2) + \frac{1}{2\epsilon_0}\int_{z_1-\sigma}^{z_1+\sigma} dz_2\, q(z_2)\left[\frac{(z_2-z_1)}{|z_2-z_1|} - \frac{(z_2-z_1)}{\sigma}\right], \tag{22}$$

$$E_d(z_1) = -\frac{1}{2\epsilon_0}\int_{z_1-\sigma}^{z_1+\sigma} dz_2\, P(z_2)\left[\frac{1}{\sigma} - \frac{(z_2-z_1)^2}{\sigma^3}\right]. \tag{23}$$

For $[\sigma/2 \leqslant z_1 \leqslant 3\sigma/2]$ the integrations have to stop at $\sigma/2$, where all densities drop to zero: $\int_{z_1-\sigma}^{z_1+\sigma} \to \int_{\sigma/2}^{z_1+\sigma}$.

In all equations above $P(z)$ is the z component of the mean polarization vector

$$\mathbf{P}(z) = \frac{1}{4\pi}\int d\Omega\ \boldsymbol{\mu}(\theta)\ \rho_d(z,\theta), \tag{24}$$

$$P(z) = \tfrac{1}{3}\,\mu\rho_d^B h_d^1(z). \tag{25}$$

The first three terms of Eq. (20) are the solution of Poissons equation for the z-dependent charge density $q(z) \equiv \Sigma_{\alpha=+,-} q_\alpha \rho_\alpha(z)$ with $\varphi_q(\infty) = 0$ and $\partial\varphi_q/\partial z\,|_{z=0} = -\epsilon_0^{-1}\omega$. The surface charge density ω of the electrode is left explicitly as a parameter in the calculation. Charge neutrality requires

$$\int_0^\infty dz\, q(z) = -\omega\ . \tag{26}$$

The last term in Eq. (20) subtracts the potential at the center z_1 of the excluded sphere with charge $q(z_2)$. Analogously one can understand the terms in Eq. (21). The boundary conditions for the Poisson solution are $\varphi_d(\infty) = 0$ and $E_d(\infty) = 0$.

The electric field in Eq. (19) is not the derivative of the potentials in Eq. (18), because a derivative with respect to the center of the sphere moves the sphere around while the field for a fixed distribution around the sphere is needed. So the fields must be summed explicitly and are recognized in Eq. (22) as the derivatives of the Poisson equation contributions of Eq. (20) minus the field at the center of a sphere with charge $q(z_2)$.

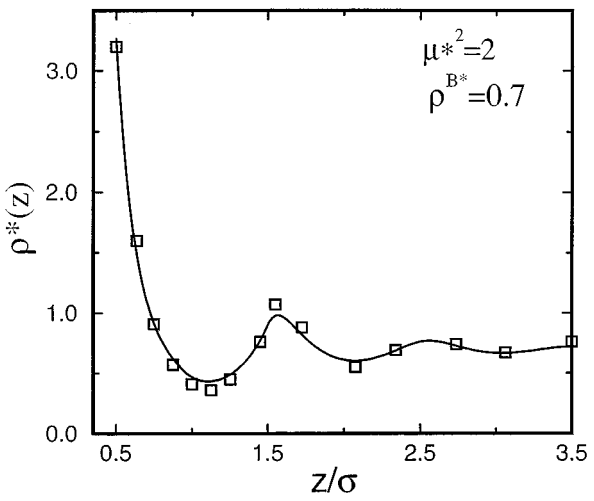

FIG. 1. The density profile for a hard sphere dipolar fluid at the uncharged wall: RHNC (solid line) and MC result (□) of Ref. 10.

A plane with constant normal polarization has no field outside, therefore only $P(z)$ from $[z-\sigma, z+\sigma]$ contributes to Eq. (23). Because of the difficult singularity of the dipole field[56] only direct integration of the field contributions at the center of the cavity over the slab with polarization $P(z)$ gives an unambiguous result, which can then also be obtained from the volume charge $-\mathrm{div}\mathbf{P}(z)$ and the surface charge $\mathbf{n}\cdot\mathbf{P}(z)$.

In order to derive integral equations for the coefficients of the expansion of the dipole density [see Eq. (12)] we use the method of Fries and Patey[35] without additional approximations needed in LHNC[33] or QHNC.[34] A differentiation with respect to θ (z differentiation for the $l=0$ coefficient) removes the logarithm function on the left-hand side of Eq. (17) and using orthogonality relations of Legendre polynomials we obtain integral equations for all coefficients of the dipole density expansion. The system of integral equations is then solved iteratively for all $\rho_d^l(z)$ ($l = 0 \ldots l_{\max}$) coefficients as well as for $\rho_+(z)$ and $\rho_-(z)$.

IV. THE STRUCTURE OF HARD SPHERE DIPOLES NEAR THE PLANAR ELECTRODE

First we solve Eqs. (17) setting the densities of the ions zero. Then the electric field due to the charge density ω on the electrode is not screened, but is only weakened due to the dielectric constant of the dipolar liquid. We therefore have as boundary conditions that the electric field, the density, and the orientation of the dipoles becomes constant in the bulk at large distances from the surface, while the electric field directly at the electrode is $\epsilon_0^{-1}\omega = E(z=0)$.

A. The uncharged electrode

When the electrode is uncharged there is no preference of the dipole polarity, the symmetry relation $\rho_d(z,\theta) = \rho_d(z,\pi-\theta)$ applies and consequently the expansion of $\rho_d(z,\theta)$ according to Eq. (12) contains only even Legendre functions. Therefore $E_z(z_1) = 0$ according to Eq. (23) vanishes for all z_1.

This article is copyrighted as indicated in the article. Reuse of AIP content is subject to the terms at: http://scitation.aip.org/termsconditions. Downloaded to IP:

TABLE II. Both sides of the contact theorem [Eq. (28)].

$\mu^{\star 2}$	$\rho_d^{\star}(z=\sigma/2)/\rho_d^{\star B}$	p/p_{id}
0	5.74	5.71
2	4.67	4.22
3	3.99	3.33

In Fig. 1 we compare our calculated dipole density

$$\rho_d(z)=\frac{1}{4\pi}\int \rho_d(z,\theta)\, d\Omega=\rho_d^0(z) \tag{27}$$

obtained for the bulk density $\rho_d^{B*}=0.7$ and dipole strength $\mu^{*^2}=2$ with simulation results from Ref. 10.

The wall-particle bridge function [Eq. (8)] is included in Eq. (17) as an additional repulsive surface potential. The agreement with the computer simulation is very good. Our calculated density profile shows the proper layering and the correct contact value is achieved. We have checked the contact value theorem

$$\frac{\rho_d^*(z=\sigma/2)}{\rho_d^{B*}}=\frac{p}{p_{id}}\,, \tag{28}$$

calculating the pressure p by the virial equation using bulk RHNC correlation functions for a density ρ_d^{B*}.

Table II compares the sides of Eq. (28) at $\rho_d^{B*}=0.7$ for three dipole strengths. The pressure and the contact value of $\rho_d(z)^*$ decreases for stronger dipole moments because on average the dipole interaction is attractive. With the reduction of the contact value of $\rho_d(z)^*$ and pressure we find also a slight decrease of the layered ordering.

Near the surface the dipolar liquid is ordered with respect to the orientation. The expansion coefficients of $\rho_d(z,\cos\theta)$ show a lot of structure (cf. Fig. 2). In Fig. 3 we show a contour plot of the probability of orientation $\rho_d(z,\cos\theta)/2\rho_d(z)$. Preferred orientation is indicated by values larger than 0.5. The contours encircle the maxima. Near the surface the dipoles are orientated preferentially parallel to

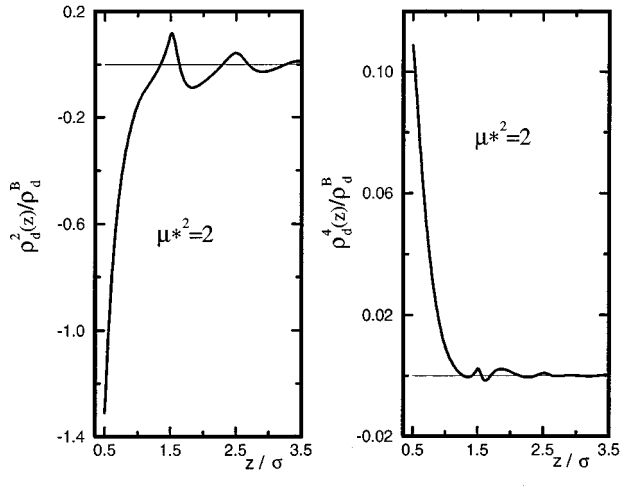

FIG. 2. The expansion coefficients of the dipole density [Eq. (12)] for $\rho^{B*}=0.7$.

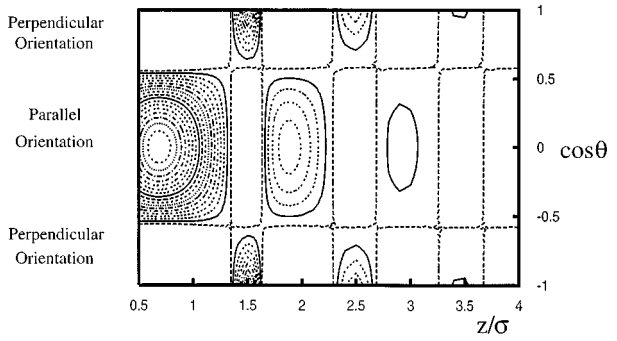

FIG. 3. Contour plots around the maxima (>0.5) of $\rho_d(z,\cos\Theta)/2\,\rho_d(z)$. The first layer near $z=0.5\ \sigma$ is orientated parallel to the wall, while the following layers at $z=1.5\ \sigma$,2.5 σ,3.5 σ are orientated perpendicular to the wall.

the surface ($\cos\theta=0$). This is the result of image forces which can be understood by a continuous medium argument. The dipoles are in a fluid of high dielectric constant facing an electrode with an effective dielectric constant 1. At such a boundary the dipoles see image charges of the same sign. Then the parallel orientation of the contact dipole with its image dipole is energetically more favorable. But the second, third, and fourth layer prefer the normal orientation. It is rather probable that these dipoles form chains. In the low density regions between the layers (at $z=2.0,3.0$), the dipoles parallel to the surface probably close rings to minimize the stray fields.

The results at the uncharged electrode compare favorably with earlier RHNC[57,58] and LRHNC[44] results and also with the results of Ref. 40 obtained at a curved surface. Without external bias the differences are small. This changes for the charged surface.

B. The charged electrode

Again for $\rho_d^{B*}=0.7$ we calculated the dipole structure for several positive surface charge densities ω and the two dipole interaction strengths $\mu^{*^2}=2$ and $\mu^{*^2}=3$. We have chosen these parameters to allow a direct comparison with the calculations of Ref. 40 where a macroion represents the charged electrode. There the charge is Ne on a sphere of diameter $2R=30\sigma$ (e elementary charge, $\sigma=2.8$ Å). We choose $\omega^*=\omega\sigma^2/e$ with the surface charge density ω. Table III compares N,ω, and ω^* and also gives the electric field at the surface. We remind that in electrochemical experiments

TABLE III. Relations between charge parameters and the external field. N is the number of elementary charges e on the macroion (Ref. 40).

N	$\omega^{\star}$	$\omega(\mathrm{C/m^2})$	$E_0(\times 10^{10}\ \mathrm{V/m})$
28.27	0.01	0.020	0.226
56.55	0.02	0.041	0.463
63.00	0.0223	0.046	0.520
84.82	0.03	0.061	0.689
108.0	0.0382	0.078	0.881
113.0	0.04	0.082	0.926
126.0	0.045	0.092	1.039

This article is copyrighted as indicated in the article. Reuse of AIP content is subject to the terms at: http://scitation.aip.org/termsconditions. Downloaded to IP:

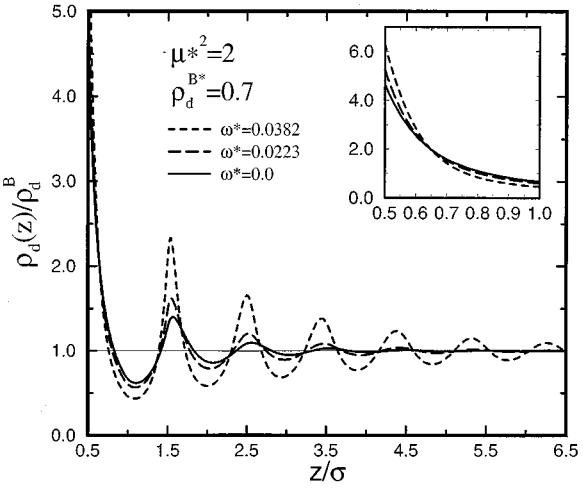

FIG. 4. The dipole density $\rho_d(z)$ for different electrode charges $\omega^\star$. The inset shows $\rho_d(z)/\rho_d^B$ near contact.

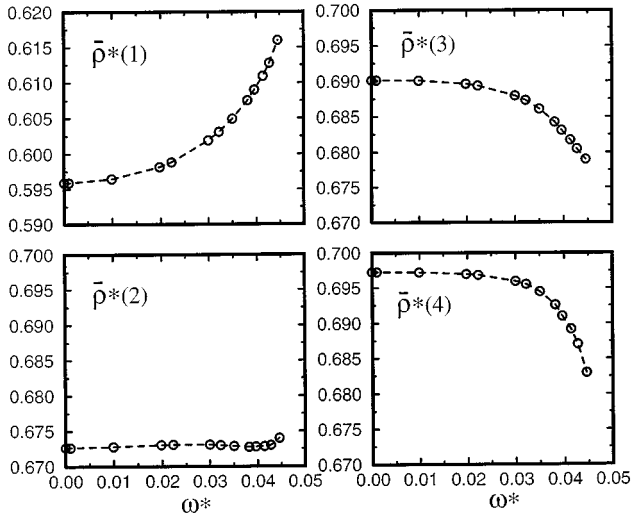

FIG. 6. Density per layer [Eq. (30)] for the first four layers ($\rho_d^{B\,\star}=0.7$, $\mu^{*2}=2$).

0.25 C/m^2 is already a very large surface charge density[59] and fields of strength 4 V/Å are the highest achievable in field ion microscopes.

In Fig. 4 we plot the dipole density $\rho_d(z)/2\rho_d^B$. We see the increased layered order with increased surface field. The increased contact value results from the dipole attraction in the field gradient. We therefore expected an increase of the dipole surface excess

$$\Gamma^*=\sigma^2\int_0^L[\rho(z)-\rho^B]dz. \tag{29}$$

To our surprise Fig. 5 shows that dipoles are expelled from the surface region when charging the electrode. Figure 6 gives more insight by monitoring the density of dipoles per layer:

$$\bar\rho^*(i)=\bar\rho^*[z=(i-0.5)\sigma]=\frac{1}{\sigma}\int_{(i-1)\sigma}^{i\sigma}\rho^*(z)\,dz\ . \tag{30}$$

Only in the first layer are the dipoles attracted; further away from the electrode the density $\bar\rho^*(i)$ is reduced. When the external field forces the dipoles to be parallel, their mutual interaction is unfavorable and they lower their density, if not a strong field gradient attracts them. According to Fig. 4, especially the regions around $z=1\sigma$ and 2σ between the "chain positions" 0.5σ,1.5σ,2.5σ,..., where without an external field the dipoles lie parallel to the surface (cf. Fig. 3), are emptied. The density in the second layer nicely demonstrates the competition between external attraction and mutual repulsion. The density in all layers near the surface is smaller than $\rho_d^{B*}=0.7$ in the bulk. In stronger electric fields the layered order extends deep into the liquid (Figs. 4 and 8). This is one aspect, in which the results at the curved surface ($2R=30\sigma$)[40] differ from ours, because their external field still decays like r^{-2}. We demonstrate in Fig. 7 the faster

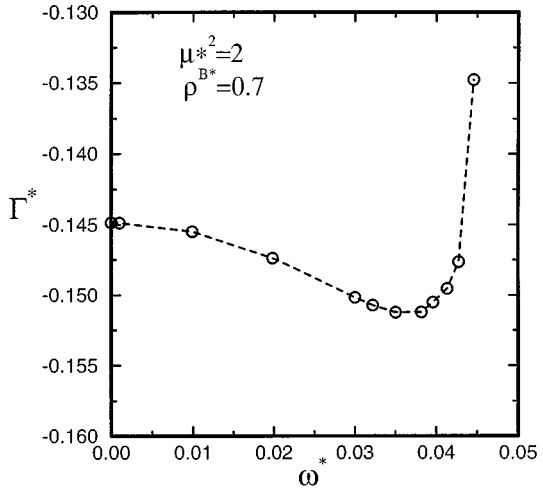

FIG. 5. The surface excess Γ_d of dipoles [Eq. (29)] vs surface charge.

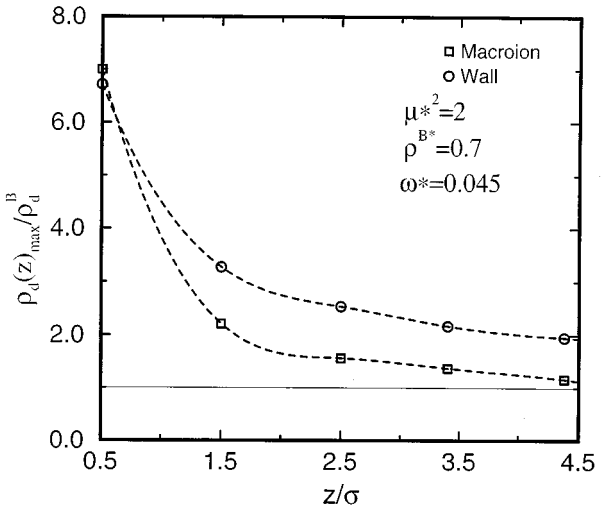

FIG. 7. Decay of the density maxima near a macroion (Ref. 40) and in front of a planar wall.

This article is copyrighted as indicated in the article. Reuse of AIP content is subject to the terms at: http://scitation.aip.org/termsconditions. Downloaded to IP:

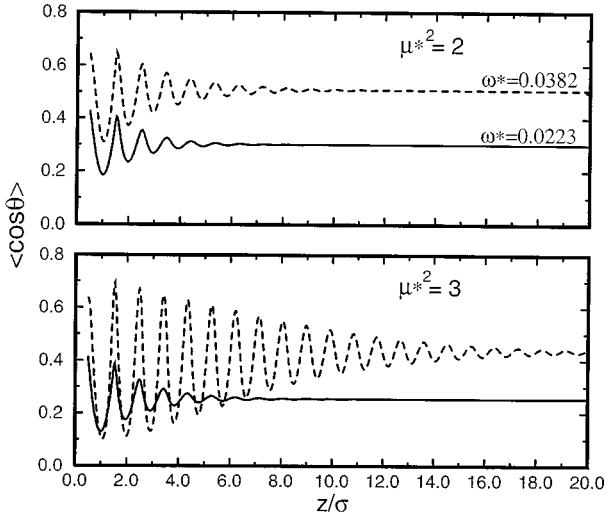

FIG. 8. The average orientation $\langle \cos \Theta \rangle$ vs distance z from the electrode.

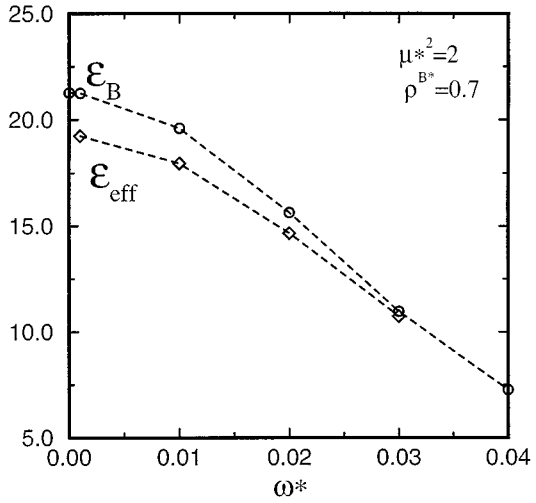

FIG. 10. The bulk dielectric constant ϵ_B decreases with increasing surface charge $\omega^\star$ due to saturation. The same is shown for the ϵ_{eff} [Eq. (38)].

decay of the density maxima in the layers for the highest available external field.

It is interesting to compare the orientational structure for two different dipole strengths in Fig. 8. The peaks of orientation parallel to the field are at the maxima of density underlining the notion of "head to tail chains." For $\mu^{*2}=2$ simply the average value of the orientation grows with growing field. For $\mu^{*2}=3$ at the first six density minima between the layers the average orientation goes more towards parallel with respect to the surface (orthogonal to the field), when increasing the surface charge. Seeing the whole distribution $\rho_d(z,\cos\theta)/2\rho_d(z)$ in Fig. 9 we learn that for the weaker mutual interaction $\mu^{*2}=2$ everywhere the dipoles follow the external field increasing their orientation towards $\cos\theta=1$, though much more strongly in the "chain positions" $z=0.56\sigma$ and 1.44σ (these z values are chosen from an analogous plot in a simulation[40]). For the stronger mutual interaction $\mu^{*2}=3$, the dipoles at $z=0.96\sigma$ and $z=1.12\sigma$, which are no "chain positions," are obviously forced parallel to the surface by the mutual interaction, even more so when the "chain" alignment is increased going from $\omega^*=0.0223$ to $\omega^*=0.0382$ [see Fig. 9(c), $\mu^{*2}=3$]. This leads to the deeper minima of $\langle\cos\theta\rangle$ in Fig. 8 for $\mu^{*2}=3$.

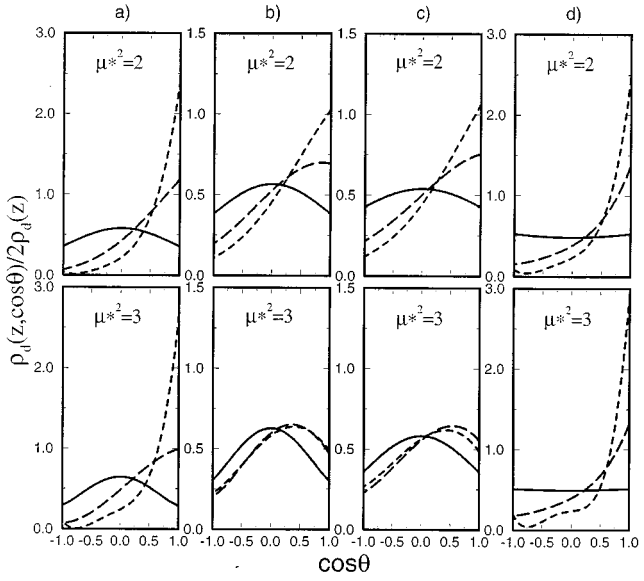

FIG. 9. The angular distribution $\rho_d(z,\cos\theta)/2\rho_d(z)$ vs $\cos\theta$ for four distances near the surface: a) $z=0.56\,\sigma$, b) $z=0.96\,\sigma$, c) $z=1.12\,\sigma$, d) $z=1.44\,\sigma$. The surface charges are $\omega^*=0$ (solid line), $\omega^*=0.0223$ (long dashed), $\omega^*=0.0382$ (short dashed).

It is also of interest to use the notion of dielectric function ϵ, because all previous double layer models have used it. With a polarization $P(z)$ we get the inner electric field from the solution of Poisson's equation

$$E(z)=\frac{\omega-P(z)}{\epsilon_0}=\frac{1}{\epsilon}E^{\text{ex}}=\frac{1}{\epsilon\epsilon_0}\,\omega\ . \tag{31}$$

For the limiting values inside the liquid, we derive the bulk dielectric constant ϵ_B from $\epsilon_B^{-1}=\epsilon_0\,(\partial E_B/\partial\omega)=1-\partial P_B/\partial\omega$. Taking the derivative shows us a dependence of ϵ on the electric field or polarization. In Fig. 10 we demonstrate the strong tendency to saturation of our orientational polarizability. The value $\epsilon_B=21.25$ for $\omega^*=0$ is close to the simulation result $\epsilon_B=16$[10] and $\epsilon_B=20$ of another bulk integral equation calculation[44,60] for these model parameters. The small difference is due to inconsistencies introduced by the approximations.

Another path to the bulk dielectric constant ϵ_B is its derivation from the local electric field within the cavity of each dipole, which is calculated in Eq. (23) in order to determine the potential energy of a dipole. When $P(z)$ has reached its constant limiting bulk value P_B, Eq. (23) plus the external field yields the local electric field

$$E^B_{\text{loc}}=\frac{1}{\epsilon_0}(\omega-\tfrac{2}{3}P_B)\ . \tag{32}$$

This article is copyrighted as indicated in the article. Reuse of AIP content is subject to the terms at: http://scitation.aip.org/termsconditions. Downloaded to IP:

P_B is related to the inner field E and the external field $E_0=\epsilon_0^{-1}\omega$ according to

$$P_B=(\epsilon_B-1)\epsilon_0 E=\frac{\epsilon_B-1}{\epsilon_B}\,\epsilon_0 E_0=\frac{\epsilon_B-1}{\epsilon_B}\,\omega\ . \tag{33}$$

We therefore can find ϵ_B from the relation between the local field and the surface charge:

$$E^B_{\rm loc}=\frac{\omega}{\epsilon_0}\left(1-\frac{2\,\epsilon_B-2}{3\,\epsilon_B}\right)=\frac{\epsilon_B+2}{3\epsilon_B}\left(\frac{\omega}{\epsilon_0}\right)\ . \tag{34}$$

We get here the field according to Clausius–Mosotti, because the medium is homogeneously polarized around the cavity in Eq. (23). We determine ϵ_B again from the derivative of Eq. (34) because ϵ_B is field dependent:

$$\frac{\partial E^B_{\rm loc}}{\partial\omega}=\frac{1}{\epsilon_0}\,\frac{\epsilon_B+2}{3\,\epsilon_B}\ . \tag{35}$$

We find the same values for $\epsilon_B(\omega)$ as from Eq. (31) (cf. Fig. 10).

If we consider the capacitance of two electrodes with the dipolar liquid in between, we get an information about the average ϵ in the whole boundary layer. Because also here ϵ depends on the external field, we evaluate the differential capacitance

$$C_d^{-1}=\frac{\partial\psi_0}{\partial\omega} \tag{36}$$

with the potential drop $\psi_0=\psi(z=0)-\psi(L)$ calculated from

$$\psi(z)=\int_z^L E(z)dz=\frac{1}{\epsilon_0}\left(\omega(L-z)-\int_z^L P(z')dz'\right) \tag{37}$$

and compare it with the capacitance $C=\epsilon\epsilon_0/L$ derived for a plate condensator to obtain

$$\epsilon_{\rm eff}^{-1}=1-\frac{\partial}{\partial\omega}\left\{\frac{1}{L}\int_0^L P(z)dz\right\}\ . \tag{38}$$

The effective $\epsilon_{\rm eff}$ obtained from Eq. (38) can be compared with the bulk values ϵ_B for different surface charges in Fig. 10. The smaller values for the average ϵ in the total capacitor indicates that near the surface the polarizability is decreased due to structural restrictions and to stronger saturation in higher fields.

We have tried to come close to a local dielectric function $\epsilon(z)$ or polarizability $\chi(z)$. This is not straightforward, because the inner field and the polarization show strong oscillations and even change sign near the surface due to the point dipole model. If we use the average polarization per layer

$$\bar P(z)=\frac{1}{\sigma}\int_{z-\sigma/2}^{z+\sigma/2}P(z)dz \tag{39}$$

we get a smooth monotonous result. We therefore write

$$\bar P(z)=(\epsilon(z)-1)\epsilon_0 E(z)=\frac{\epsilon(z)-1}{\epsilon(z)}\,\epsilon_0 E_{\rm ext}=\frac{\epsilon(z)-1}{\epsilon(z)}\,\omega \tag{40}$$

and

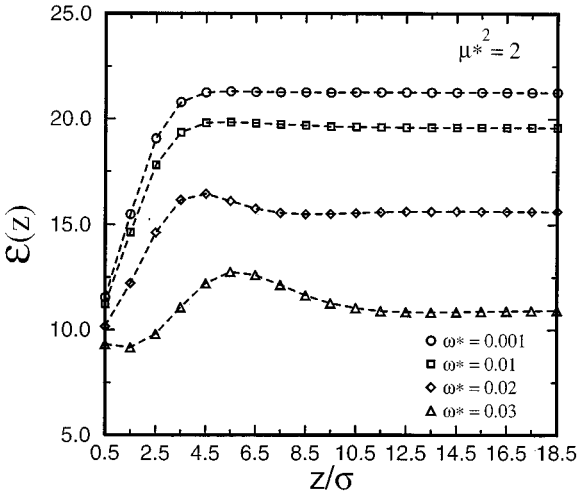

FIG. 11. The dielectric function per layer [Eq. (41)].

$$\frac{\partial\bar P}{\partial\omega}(z)=\frac{\epsilon(z)-1}{\epsilon(z)}\Rightarrow\ \epsilon^{-1}(z)=1-\frac{\partial\bar P}{\partial\omega}(z) \tag{41}$$

which according to Eq. (38) could also be derived via a concept of a sequence of capacitors. The $\epsilon(z)$ from Eq. (41) is plotted in Fig. 11 for different ω^*. We see that $\epsilon(z)$ near the surface is always lower than in the bulk. The dipoles are oriented in a certain structure and cannot so easily follow the field. The combination of orientation and change in density of dipoles can even lead to a maximum in $\epsilon(z)$.

V. DISTRIBUTION AND ORIENTATION OF IONS AND DIPOLES NEAR THE PLANAR ELECTRODE

We now determine the densities $\rho_+(z),\rho_-(z)$ for the ions and $\rho_d(z,\theta)$ for the dipoles from Eqs. (16) and (17). We expand $\rho_d(z,\theta)$ up to $l=4$ [see Eq. (12)]. The required direct correlation functions $c_{ij}(r_{ij})$ are calculated in the RHNC approximation with expansions in spherical invariants up to $l_{\rm max}=2$.[54,61] We choose $\mu^{*2}=2$ and the total density $\rho_T^*=\rho_+^*+\rho_-^*+\rho_d^*=0.7$ in the bulk as in the previous section.

The two new model parameters are the ionic charge and concentration. We use a concentration of 0.1 molar (0.1 M) typical for an electrolyte, which gives an ion concentration $c=(\rho_++\rho_-)/\rho_T=0.0036$ and $\rho_+^*=\rho_-^*=0.001\,26$. Some calculations for smaller concentrations are also presented. The ionic charge $\pm q$ determines the interactions and is measured by $q^{*2}=q^2/(\sigma kT)$. We use $q^*=6$ and $q^*=8$. At larger ionic interactions, the hard sphere ion-dipole mixture becomes unstable with respect to demixing.[61,62] This is unfortunate, because $q^*=8$ means only 0.57 of an elementary charge for a hard sphere diameter of $\sigma=2.8$ Å and temperature $T=300$ K. If one does not like to face these limitations of the model one can interpret the system as fully charged ions at extremely large temperature.[44] Our bulk electrolyte is chosen well in the stable region of the phase diagram. For large external fields the concentration of ions near the elec-

This article is copyrighted as indicated in the article. Reuse of AIP content is subject to the terms at: http://scitation.aip.org/termsconditions. Downloaded to IP:

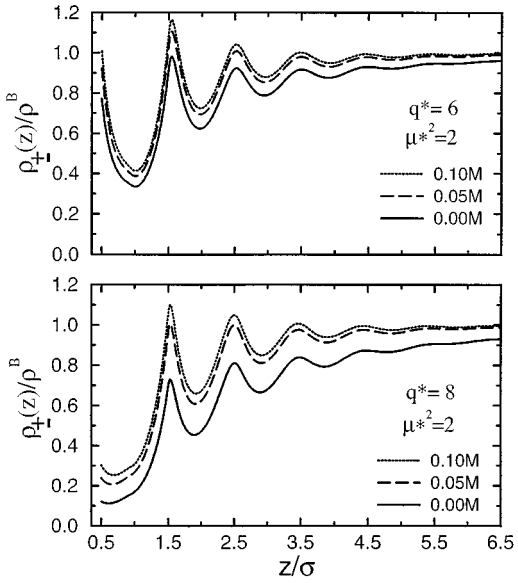

FIG. 12. The density profiles of the ions in the ion-dipole mixture near the uncharged electrode for three concentrations.

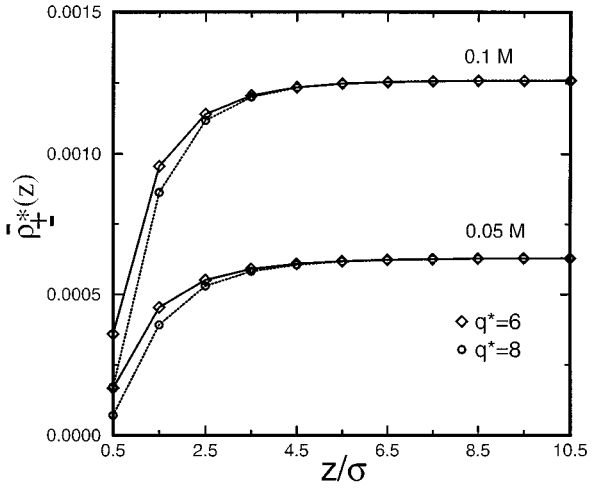

FIG. 13. The ion density per layer near the uncharged wall.

trode is strongly enhanced and we finally see a behavior of the ion distribution, which is probably due to this phase instability.

A. The uncharged electrode

In Fig. 12 we show the ionic density profile $\rho_\alpha(z)/\rho_\alpha^B$ for both ion species at the uncharged electrode. The concentration 0.0 M means infinite dilution neglecting all ion-ion correlations in Eqs. (16) and (17). In spite of the low ionic concentrations, we see here a density structure which is introduced by the solvent molecules. If we treat the ions as a gas in a homogeneous dielectric medium (primitive model), the contact value is always very much higher than all other densities[16] and very little structure appears. Here the ions are excluded from the first layer of the electrolyte, more so for higher ion charge. We can understand this by a stable solvation shell and/or by a repulsive image interaction of the charge in the highly dielectric medium in front of the nonpolarizable region with $\epsilon=1$. The image repulsion makes even the peaks in the second and third layer smaller than the bulk density for $q^*=8$ and 0.0 M.

Also the average ion density in each layer obtained from Eq. (30) is much lower than in the bulk (Fig. 13). Another effect dragging the ions to the interior is the reduction of the ion chemical potential in the Debye–Hückel screening cloud, which is fully developed only further away from the surface. The dipole density near the surface slightly increases with increasing ion concentration and ionic charge, compared to the density of the pure dipoles. Obviously the solvation of the ions disturbs the optimal arrangement of the dipoles, reduces their average mutual attraction, and increases the pressure. Also the probability of orientation parallel to the surface in the contact layer (see Fig. 3) is reduced proportional to ion concentration and charge q^*, because the solvation of ions which mainly are placed in the second layer around 1.5σ (according to Fig. 12) will turn some dipoles normal to the surface.

B. The charged electrode

In this section we present results for a 0.1 M concentrated electrolyte ($\rho_+^*=\rho_-^*=0.001\,26$, $c=\rho_+ +\rho_-/\rho_T=0.0036$) with total density $\rho_T^*=0.7$, dipole strength $\mu^{*2}=2$, and ionic charges $q^*=6$ and $q^*=8$. The largest surface charges are again in the range of high experimental charges. Because we find some instability in the electrolyte with $q^*=8$, which limits us in finding convergent solutions, the extremal surface charge is a bit smaller than for $q^*=6$.

In Fig. 14 we show the ion density per layer [Eq. (30)] for the negative ions at the positive electrode. We see that the solvation keeps the ions away from the first layer, more so for the higher ionic charge, where the solvation is obviously more stable.

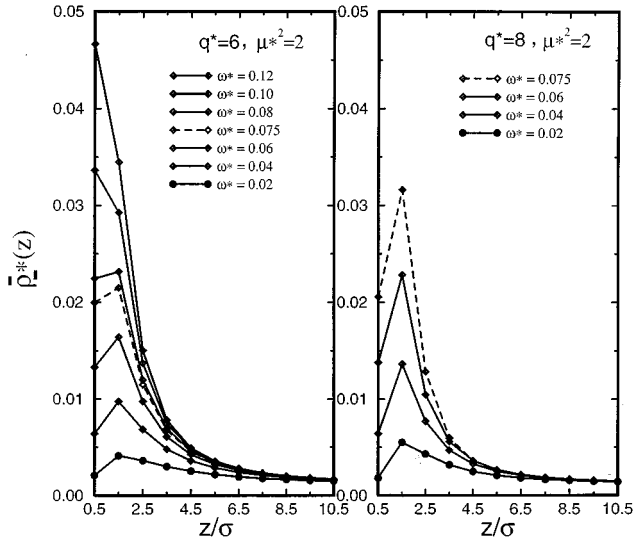

FIG. 14. The density of negative ions per layer near the positively charged electrode for ion concentration 0.1 M.

This article is copyrighted as indicated in the article. Reuse of AIP content is subject to the terms at: http://scitation.aip.org/termsconditions. Downloaded to IP:

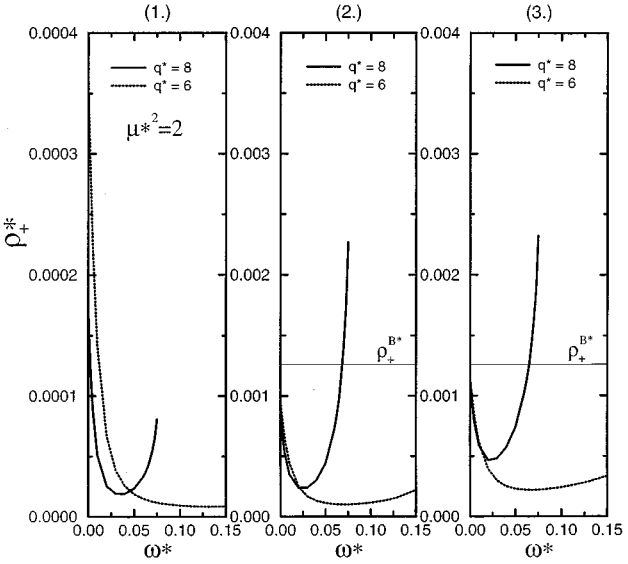

FIG. 15. The density of positive ions in the first three layers vs surface charge for ion concentration 0.1 M.

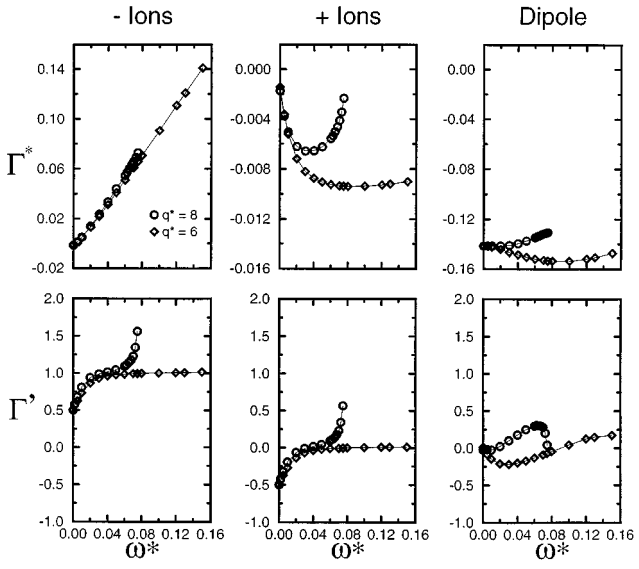

FIG. 16. The surface excess $\Gamma^{\star}$ and its derivate $\Gamma^{\star\prime}$ with respect to surface charge for the ions and the dipoles.

It is also interesting to look at the density of positive ions in Fig. 15. One expects a reduction with increasing surface charge. Surprisingly this is not the case for the large ionic interaction $q^*=8$. Obviously more negative charges enter the double layer than necessary for screening the field. They partly drag their positive partners with them. The reason might be the larger tendency towards pair formation for higher ionic charges.

We can also show that the screening of the external field for $q^*=8$ is so efficient that beyond $\omega^*=0.04$ the electric field in the second and third layer decreases with growing ω^*, which brings part of the positive ions back. This cannot, however, explain the increase of ρ_+^* above the bulk value.

But after our experience with instabilities of the ion-dipole mixture[61,62] we suspect that we see an indication of a condensation of the ions on the surface. In the bulk, the system shows an instability towards condensation of the ions around concentrations of 1 molar.[62] One can only say that the electrolyte concentration is increased in the external field near the surface. In order to analyze the situation further, we look at the surface excess of the ions

$$\Gamma_\alpha = \int_0^\infty [\rho_\alpha(z) - \rho_\alpha^B] dz \ .$$

For a more drastic signal we take the derivative of Γ with respect to the electrode charge

$$\Gamma' = \frac{\partial \Gamma^*}{\partial \omega^*} \tag{42}$$

with $\Gamma^* = \sigma^2 \Gamma$ and $\omega^* = \omega \sigma^2 / q$. Because of the screening condition $q(\Gamma_- - \Gamma_+) = \omega$ the Γ' has to fullfil the relation

$$\left(\frac{\partial \Gamma_-^*}{\partial \omega^*} - \frac{\partial \Gamma_+^*}{\partial \omega^*} \right) = 1. \tag{43}$$

The Γ' are plotted in Fig. 16. For small external fields positive and negative ions contribute equally to the screening ($\Gamma' = \pm 0.5$), as the Debye–Hückel theory requires. Very soon the screening is accomplished solely by the counterions ($\Gamma'_- = 1, \Gamma'_+ = 0$). But in the system with $q^*=8$ and surface charge density around $\omega^*=0.04$ suddenly both numbers of ions start growing in the surface region. In the plot of Γ'_d for the dipoles in Fig. 16 we indeed see that the trend of increasing growth of dipole density for $q^*=8$ is suddenly reversed. When there is a condensation of the ions, the dipoles are partially replaced by the ions. We understand the initial decrease of Γ'_d for the small ion charge $q^*=6$ in the same way as explained for the pure dipolar fluid in the field of the surface charge. For the higher ion charge $q^*=8$ this trend is counterbalanced by the tendency of each ion to carry its solvation shell into the double layer.

In addition to densities we get the information about the dipole orientation and polarization in the double layer. The order of the dipoles and related effects are smaller than for the pure dipolar fluid as shown in Fig. 9, because the field is strongly screened.

The overall result of all these distributions is the differential capacitance C_d of the double layer

$$C_d^{-1} = \frac{d\psi_0}{d\omega} \ , \tag{44}$$

where $\psi_0 = \psi(z=0) - \psi(\infty)$ is the potential drop across the double layer

$$\psi_0 = -\frac{1}{\epsilon_0} \int_0^\infty z \ q(z) \ dz - \frac{1}{\epsilon_0} \int_0^\infty P(z) \ dz. \tag{45}$$

We compare our result for C_d (see Fig. 17) with the Gouy–Chapman values and an RPM evaluation. We use in both cases a dielectric constant $\epsilon = 19$ determined in a RHNC calculation for the bulk ion-dipole mixture with our parameters.[61] For a fair comparison also in these continuum solvent models we have to leave an empty selvedge with

This article is copyrighted as indicated in the article. Reuse of AIP content is subject to the terms at: http://scitation.aip.org/termsconditions. Downloaded to IP:

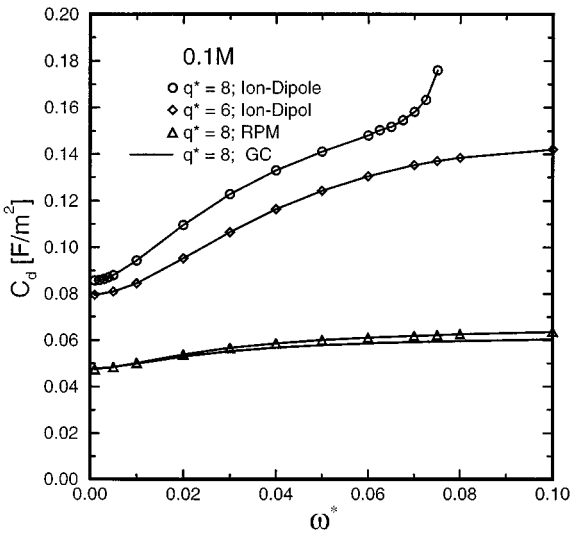

FIG. 17. The differential capacitance.

$\epsilon=1$ between $z=0$ and $z=\sigma/2$, because in our model with hard sphere dipoles the polarization starts at $z=\sigma/2$. The values for the microscopic model are larger than from RPM and GC. In our model the dielectric response is not constant throughout the double layer, but decreases near the wall. In addition, the ionic packing is determined by the solvent structure. In view of these facts, it is remarkable how large the differential capacitance, how good the screening is compared to the continuum models. The screening charge is probably just dragged closer to the electrode, because the electric field is less weakened due to the smaller dielectric function near the surface.

For the electrolyte with $q^*=8$ the differential capacitance is suddenly steeply growing, which is related to the suspected phase instability with respect to ion condensation discussed in connection with Figs. 15 and 16. This is an indication of a model case for such an irregularity in the differential capacitance as recently again discussed by Partenskii and Jordan.[63] When there is an instability in the ion distribution, it may happen that for a certain increase $\Delta\omega$ in the surface charge density there could be such a redistribution of the screening charge that the potential difference towards the bulk increases very little, as in our case, or may even increase not at all ($C_d=\infty$) or even decrease ($C_d<0$). Because not the amount of charge but its distribution determines the potential drop, there is nothing mysterious about this result. We will try to investigate this case in more detail in the future.

VI. ELECTROSTRICTION

During discussions with J. P. Badiali and V. Russier we were urged to also consider electrostriction for the pure dipoles, where the field is not screened. Up to now we have reported about calculations which used a constant given bulk liquid density of $\rho^*=0.7$ as a boundary condition. We think that this assumption is justified for studying all the qualitative features we have analyzed. Experimentally, this condition would be applicable to a completely closed parallel capacitor of very large area such that essentially all the available liquid sees the same bulk field.

When a capacitor dives into a liquid, usually the liquid in the field is connected to a bath of liquid without a field. Then the liquid in the field increases its density with increasing field because the field lowers the chemical potential of the molecules, which then flow in from the bath. The increase of the density can be estimated in the following way:

We start from the exact thermodynamic relation for the chemical potential at the macroscopic inner field intensity E:[64]

$$\mu(T,E,\rho)=\mu(T,0,\rho)-\frac{\epsilon_0}{2}\int_0^{E^2}\left(\frac{\partial\epsilon}{\partial\rho}\right)_{T,E}dE^2. \tag{46}$$

$\partial\epsilon/\partial\rho$ is positive and we approximate it independently of the field by

$$\frac{\widetilde{\partial\epsilon}}{\partial\rho^*}\approx\frac{1}{\delta\rho^*}[\epsilon(\rho^*+\delta\rho^*)_{T,E=0}-\epsilon(\rho^*)_{T,E=0}]. \tag{47}$$

We calculated ϵ for $\rho^*=0.7$ and $\rho^*=0.701$.

Because our system is coupled to the bath with $\mu(T,0,\rho_0)$, $\mu(T,E,\rho)=\mu(T,0,\rho_0)$, which is achieved by increasing the density by $\Delta\rho$:

$$\mu(T,0,\rho_0+\Delta\rho)-\mu(T,0,\rho_0)=\frac{\epsilon_0}{2}\left(\frac{\widetilde{\partial\epsilon}}{\partial\rho}\right)E^2. \tag{48}$$

The following further approximations are used:

$$\begin{aligned}\mu(T,0,\rho_0+\Delta\rho)-\mu(T,0,\rho_0)&=\int_{\rho_0}^{\rho_0+\Delta\rho}\frac{\partial\mu}{\partial\rho}\,d\rho\\&=\int_{\rho_0}^{\rho_0+\Delta\rho}\frac{1}{\rho}\frac{\partial p}{\partial\rho}\,d\rho\\&\approx\left(\frac{1}{\rho}\frac{\partial p}{\partial\rho}\right)_{\rho_0}\Delta\rho\end{aligned} \tag{49}$$

with

$$\begin{aligned}\beta\frac{\partial p}{\partial\rho}&=-\frac{\beta V^2}{N}\left(\frac{\partial p}{\partial V}\right)_N\\&=\frac{\beta}{\rho}\left(-\frac{1}{V}\frac{\partial V}{\partial p}\right)^{-1}\\&=\frac{1}{\rho\,kT\,\chi}\\&=\left(1+\sqrt{4\pi}\,\rho\int_0^\infty dr\,r^2\,h_{dd}^{000}(r)\right)^{-1}\end{aligned} \tag{50}$$

and

$$E\approx\frac{E_0}{\epsilon(\rho_0,E_0)}=\frac{\omega}{\epsilon_0\,\epsilon(\rho_0,\omega)}\,. \tag{51}$$

Finally with reduced quantities $\Delta\rho^*$ is given by

This article is copyrighted as indicated in the article. Reuse of AIP content is subject to the terms at: http://scitation.aip.org/termsconditions. Downloaded to IP:

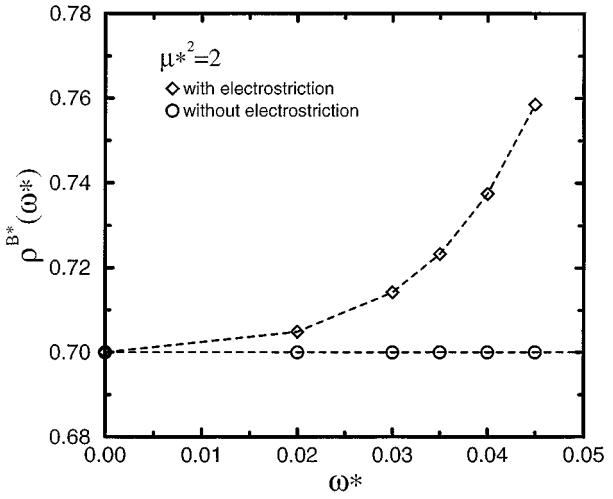

FIG. 18. Increase of the bulk density due to electrostriction.

$$\frac{\Delta\rho^*}{\rho_0^*}=\frac{\epsilon}{2}\frac{\partial\widetilde{\epsilon}}{\partial\rho^*}\left(\frac{\omega^*}{\epsilon_0\ \epsilon(\rho_0^*,\omega^*)}\right)^2\ (\rho_0\ kT\ \chi)\ \frac{e^2}{\sigma\ kT}\ . \tag{52}$$

Our calculations yield $\partial\widetilde{\epsilon}/\partial\rho^*=74$ and $\rho\ kT\ \chi=0.067$.

We have now calculated with the increased density $\rho^*(\omega^*)=\rho^*(0)+\Delta\rho^*(\omega^*)$ as the bulk limit. We first plot in Fig. 18 the increase of ρ^* as a function of the surface charge density ω^*. We find an increase of ρ by 8.3% for the largest fields used. At each z the density grows, but faster in the first layer and less in the third and fourth layers than in the bulk. This is shown in Fig. 19, where we plot $\widetilde{\Delta\rho^*}$:

$$\widetilde{\Delta\rho^*}(i)=\frac{1}{\sigma}\int_{(i-1)\sigma}^{i\sigma}\rho^*(z,\omega^*)\ dz-\rho^{B*}(\omega^*). \tag{53}$$

Therefore the arguments from Sec. II about attraction in the inhomogeneous field in the first layer and mutual repulsion of dipoles forced parallel in ordered layers are still applicable and give even larger effects for higher densities. The surface excess $\Gamma^*(\omega^*)$, which is always negative, is not much changed for the electrostriction case, when Γ is calculated properly with respect to the bulk $\rho^*(\omega^*)$. For the electrolyte with ions there is no electrostriction because screening makes the field zero in the bulk.

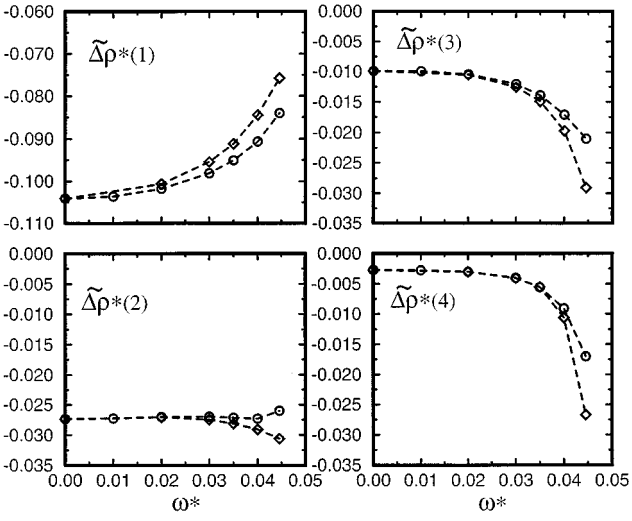

FIG. 19. The density changes in the first four layers [Eq. (53)]: with (◇) and without (○) electrostriction.

VII. CONCLUSIONS

For the electrolyte model of hard sphere ions and hard sphere dipoles the particle distributions and orientations near a planar electrode under bias conditions have been calculated here for the first time by solving the integral equations without linearization. We solve the Euler equations from density functional theory, approximated to the HNC equivalent and amended by a "bridge function," which is an effective repulsive potential of the electrode. The required particle–particle correlations are taken from RHNC bulk calculations.

The calculated densities give the following insight into the structure of the double layer. For the pure dipolar fluid the density near the uncharged electrode is decreased, relative to the bulk liquid, because the dipole interactions are attractive on average. When charging the electrode, the dipoles are attracted in the first contact layer due to the large field gradient. But in the third and fourth layer the density is decreased so that the surface excess, which is already negative before charging, is actually decreasing. We understand this unexpected result by the mutual repulsion of dipoles, which are forced parallel by the external field. The apparent chain structure is strengthened in the external field. The dielectric function ϵ (Fig. 11) is smaller near the surface than in the bulk because the dipoles are obviously bound into a structure and less free to respond to the field. For higher external fields, ϵ decreases everywhere due to onset of saturation of the orientational polarizability. When the ions are added, they are kept away from the electrode by solvation, by image forces inside the dipolar liquid and by Debye–Hückel attraction of the ions. The cohesion of the dipoles is weakened, they increase their density near the electrode. When the electrode is charged, the field is so strongly screened that the density of coions behaves nonmonotonously. The differential capacitance of this model with microscopic solvent structure is higher than that of the restricted primitive model (RPM) or the Gouy–Chapman result. The reason is better screening, a more densely packed double layer due to stronger external fields at smaller dielectric constants.

One additional feature of our model is its instability for higher ionic charges and higher concentrations.[61,62] We consider this fact responsible for a "condensation" effect of the ions on to the surface at the highest surface charges, which leads to a sudden increase of the differential capacitance. This special property of our model, which simulates electrolytes with a demixing transition,[62] will be studied in more detail in the future.

ACKNOWLEDGMENTS

We are grateful for the helpful discussions with X.S. Chen, M. Kasch, M. Vossen and F. Weich as well as for the

This article is copyrighted as indicated in the article. Reuse of AIP content is subject to the terms at: http://scitation.aip.org/termsconditions. Downloaded to IP:

provision of some programs for the bulk correlation functions by X.S. Chen and M. Kasch. Discussions with J. P. Badiali, whose great hospitality in Paris is gratefully acknowledged, and with V. Russier lead us to consider Sec. VI. E. Díaz-Herrera acknowledges gratefully a grant by the Deutscher Akademischer Austauschdienst.

[1] G. Gouy, J. Phys. **9**, 451 (1910).
[2] D. L. Chapman, Philos. Mag. **25**, 475 (1913).
[3] J. Bockris and A. K. N. Reddy, *Modern Electrochemistry* (Plenum, New York, 1970), Vol. 2.
[4] D. Henderson, L. Blum, and M. Lozada-Cassou, J. Electroanal. Chem. **150**, 291 (1983).
[5] P. Nielaba, T. Knowles, and F. Forstmann, J. Electroanal. Chem. **183**, 329 (1985).
[6] R. Parsons, J. Electroanal. Chem. **59**, 229 (1975).
[7] J. P. Badiali, M. L. Rosinberg, F. Vericat, and L. Blum, J. Electroanal. Chem. **158**, 253 (1983).
[8] W. Schmickler and D. Henderson, J. Chem. Phys. **85**, 1650 (1986).
[9] S. Amokrane and J. P. Badiali, in *Modern Aspects of Electrochemistry*, edited by J. Bockris, B. E. Conway, and R. E. White (Plenum, New York, 1992), pp. 1–95.
[10] D. Levesque and J. J. Weis, J. Stat. Phys. **40**, 29 (1985).
[11] G. M. Torrie and J. P. Valleau, J. Phys. Chem. **86**, 3251 (1982).
[12] D. Henderson and L. Blum, J. Chem. Phys. **69**, 5441 (1978).
[13] D. Henderson, L. Blum, and W. R. Smith, Chem. Phys. Lett. **63**, 381 (1979).
[14] D. Henderson, F. F. Abraham, and J. A. Barker, Mol. Phys. **31**, 1291 (1976).
[15] L. Blum, J. Hernando, and J. L. Lebowitz, J. Phys. Chem. **87**, 2895 (1983).
[16] S. L. Carnie and G. M. Torrie, Adv. Chem. Phys. **56**, 141 (1984).
[17] M. Plischke and D. Henderson, J. Chem. Phys. **88**, 2712 (1988).
[18] C. Caccamo, G. Pizzimenti, and L. Blum, Phys. Chem. Liq. **14**, 311 (1985).
[19] C. Caccamo, G. Pizzimenti, and L. Blum, J. Chem. Phys. **89**, 3327 (1986).
[20] P. Ballone, G. Pastore, and M. P. Tosi, J. Chem. Phys. **85**, 2943 (1986).
[21] P. Nielaba and F. Forstmann, Chem. Phys. Lett. **117**, 46 (1985).
[22] B. D'Aguanno, P. Nielaba, T. Alts, and F. Forstmann, J. Chem. Phys **85**, 3476 (1986).
[23] T. Alts, P. Nielaba, B. D'Aguanno, and F. Forstmann, Chem. Phys. **111**, 223 (1987).
[24] R. Kjellander and S. Marcelja, Chem. Phys. Lett. **112**, 49 (1984).
[25] R. Kjellander and S. Marcelja, J. Chem. Phys. **82**, 2122 (1985).
[26] R. Kjellander and S. Marcelja, Chem. Phys. Lett. **127**, 464 (1986).
[27] M. S. Wertheim, Mol. Phys. **26**, 1425 (1973).
[28] M. S. Wertheim, Mol. Phys. **34**, 1109 (1977).
[29] J. S. Høy and G. Stell, J. Chem. Phys. **61**, 562 (1974).
[30] J. S. Høy and G. Stell, J. Chem. Phys. **72**, 1597 (1980).
[31] M. S. Wertheim, J. Chem. Phys. **55**, 4291 (1971).
[32] D. J. Isbister and B. C. Freasier, J. Stat. Phys. **20**, 331 (1979).
[33] J. M. Eggebrecht, D. J. Isbister, and J. C. Rasaiah, J. Chem. Phys. **73**, 3980 (1980).
[34] J. C. Rasaiah, D. J. Isbister, and G. Stell, J. Chem. Phys. **75**, 4707 (1981).
[35] P. H. Fries and G. N. Patey, J. Chem. Phys. **82**, 429 (1985).
[36] J. M. Caillol, Chem. Phys. Lett. **121**, 347 (1985).
[37] J. M. Caillol, D. Levesque, and J. J. Weis, Mol. Phys. **69**, 199 (1990).
[38] J. M. Caillol *et al*., Mol. Phys. **62**, 461 (1987).
[39] P. G. Kusalik and G. N. Patey, J. Chem. Phys. **88**, 7715 (1988).
[40] G. M. Torrie, A. Perera, and G. N. Patey, Mol. Phys. **67**, 1337 (1989).
[41] G. M. Torrie, P. G. Kusalik, and G. N. Patey, J. Chem. Phys. **88**, 7826 (1988).
[42] G. M. Torrie, P. G. Kusalik, and G. N. Patey, J. Chem. Phys. **90**, 4513 (1989).
[43] M. Kinoshita and M. Harada, Mol. Phys. **81**, 1473 (1994).
[44] W. Dong, M. L. Rosinberg, A. Perera, and G. N. Patey, J. Chem. Phys. **89**, 4994 (1988).
[45] D. R. Bérard, M. Kinoshita, X. Ye, and G. N. Patey, J. Chem. Phys. **101**, 6271 (1994).
[46] D. R. Bérard and G. N. Patey, J. Chem. Phys. **97**, 4372 (1992).
[47] R. Evans, Adv. Phys. **28**, 143 (1979).
[48] R. Evans, in *Fundamentals of Inhomogeneous Fluids*, edited by D. Henderson (Marcel Dekker, New York, 1992), pp. 85–175.
[49] M. Kasch, X. S. Chen, and F. Forstmann, Mol. Phys. **75**, 415 (1992).
[50] Y. Rosenfeld, Phys. Rev. A **37**, 4303 (1988).
[51] F. Lado, Phys. Rev. A **135**, 1013 (1964).
[52] F. Lado, Mol. Phys. **31**, 1177 (1976).
[53] M. Kasch and F. Forstmann, J. Chem. Phys. **99**, 3037 (1993).
[54] X. S. Chen and F. Forstmann, Mol. Phys. **76**, 1203 (1992).
[55] C. G. Gray and K. E. Gubbins, *Theory of Molecular Fluids* (Oxford University, Oxford, 1984), Vol. 1.
[56] J. D. Jackson, *Classical Electrodynamics*, 2nd ed. (Wiley, New York, 1975), Chap. 4.1.
[57] D. R. Bérard and G. N. Patey, J. Chem. Phys. **95**, 5281 (1991).
[58] M. Kinoshita and M. Harada, Mol. Phys. **79**, 145 (1993).
[59] A. Hamelin, L. Stoicoviciu, and F. Silva, J. Electroanal. Chem. **229**, 107 (1987).
[60] M. Kasch, Ph.D. thesis, Freie Universität Berlin, 1992.
[61] X. S. Chen, Ph.D. thesis, Freie Universität Berlin, 1992.
[62] X. S. Chen, M. Kasch, and F. Forstmann, Phys. Rev. Lett. **67**, 2674 (1991).
[63] M. B. Partenksii and P. C. Jordan, J. Chem. Phys. **99**, 2992 (1993).
[64] A. Sanfeld, *Introduction to the Thermodynamics of Charged and Polarized Layers* (Wiley, New York, 1968), Chap. 8.V.

This article is copyrighted as indicated in the article. Reuse of AIP content is subject to the terms at: http://scitation.aip.org/termsconditions. Downloaded to IP: